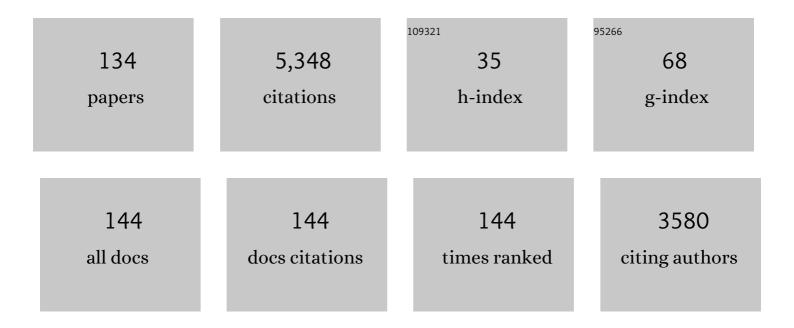
List of Publications by Year in descending order

Source: https://exaly.com/author-pdf/7006900/publications.pdf Version: 2024-02-01



LINE CLATZEL

#	Article	IF	CITATIONS
1	Decomposition in multi-component AlCoCrCuFeNi high-entropy alloy. Acta Materialia, 2011, 59, 182-190.	7.9	656
2	Microstructure and mechanical properties of selective laser melted Inconel 718 compared to forging and casting. Materials Letters, 2016, 164, 428-431.	2.6	358
3	Phase separation in equiatomic AlCoCrFeNi high-entropy alloy. Ultramicroscopy, 2013, 132, 212-215.	1.9	296
4	Mechanical and Microstructural Investigation of Nickelâ€Based Superalloy IN718 Manufactured by Selective Laser Melting (SLM). Advanced Engineering Materials, 2015, 17, 1099-1105.	3.5	218
5	Temperature dependence of the elastic moduli of the nickel-base superalloy CMSX-4 and its isolated phases. Materials Science & Engineering A: Structural Materials: Properties, Microstructure and Processing, 2001, 298, 26-33.	5.6	194
6	High-Temperature Tensile Strength of Al10Co25Cr8Fe15Ni36Ti6 Compositionally Complex Alloy (High-Entropy Alloy). Jom, 2015, 67, 2271-2277.	1.9	140
7	Measurement of the lattice misfit in the single crystal nickel based superalloys CMSX-4, SRR99 and SC16 by convergent beam electron diffraction. Acta Materialia, 1998, 46, 4395-4404.	7.9	120
8	Chemical composition measurements of a nickel-base superalloy by atom probe field ion microscopy. Materials Science & Engineering A: Structural Materials: Properties, Microstructure and Processing, 1995, 203, 69-74.	5.6	116
9	High performance environmental barrier coatings, Part I: Passive filler loaded SiCN system for steel. Journal of the European Ceramic Society, 2011, 31, 3003-3010.	5.7	115
10	Quantitative experimental determination of the solid solution hardening potential of rhenium, tungsten and molybdenum in single-crystal nickel-based superalloys. Acta Materialia, 2015, 87, 350-356.	7.9	115
11	Investigation of phases in Al23Co15Cr23Cu8Fe15Ni16 and Al8Co17Cr17Cu8Fe17Ni33 high entropy alloys and comparison with equilibrium phases predicted by Thermo-Calc. Journal of Alloys and Compounds, 2013, 552, 430-436.	5.5	112
12	Modelling and analysis of the oxidation influence on creep behaviour of thin-walled structures of the single-crystal nickel-base superalloy René N5 at 980 °C. Acta Materialia, 2010, 58, 1607-1617.	7.9	104
13	Modelling of High Temperature Oxidation of Alumina-Forming Single-Crystal Nickel-Base Superalloys. Acta Materialia, 2012, 60, 5468-5480.	7.9	98
14	New multiphase compositionally complex alloys driven by the high entropy alloy approach. Materials Characterization, 2019, 147, 512-532.	4.4	95
15	Calculations of internal stresses in the γ/γ′ microstructure of a nickel-base superalloy with high volume fraction of γ′-phase. Scripta Metallurgica, 1989, 23, 1839-1844.	1.2	94
16	Carbon nanofibre-reinforced ultrahigh molecular weight polyethylene for tribological applications. Journal of Applied Polymer Science, 2007, 104, 4173-4181.	2.6	93
17	Metallic materials for structural applications beyond nickel-based superalloys. Jom, 2009, 61, 61-67.	1.9	92
18	Calculation of the internal stresses and strains in the microstructure of a single crystal nickel-base superalloy during creep. Acta Metallurgica Et Materialia, 1993, 41, 3401-3411.	1.8	85

#	Article	IF	CITATIONS
19	Determination of heat transfer coefficient and ceramic mold material parameters for alloy IN738LC investment castings. Journal of Materials Processing Technology, 2011, 211, 181-186.	6.3	71
20	On the Path to Optimizing the Al-Co-Cr-Cu-Fe-Ni-Ti High Entropy Alloy Family for High Temperature Applications. Entropy, 2016, 18, 104.	2.2	68
21	Microstructure and Tensile Behavior of Al8Co17Cr17Cu8Fe17Ni33 (at.%) High-Entropy Alloy. Jom, 2013, 65, 1805-1814. Oxidation Behavior of	1.9	66
22	Al <sub>8</sub> Co <sub>17</sub> Cr <sub>17</sub> Cu <sub>8</sub> Fe <sub>17</sub> Ni <sub>33</sub> , Al <sub>23</sub> Co <sub>15</sub> Cr <sub>23</sub> Cu <sub>8</sub> Fe <sub>15</sub> Ni <sub>15</sub> , and Al <sub>17</sub> Co <sub>17</sub> Cr <sub>17</sub> Cu <sub>17</sub> Fe <sub>17</sub> Ni <sub>17</sub>	3.5	60
23	Compositionally Complex Alloys (Highâ€Entropy Alloys) at Elevated Temperatures in Air. Advanced Influence of oxidation on near-surface γ′ fraction and resulting creep behaviour of single crystal Ni-base superalloy M247LC SX. Materials Science & Engineering A: Structural Materials: Properties, Microstructure and Processing, 2013, 577, 179-188.	5.6	55
24	A dislocation density based material model to simulate the anisotropic creep behavior of single-phase and two-phase single crystals. International Journal of Plasticity, 2009, 25, 973-994.	8.8	52
25	Thickness influence on creep properties for Ni-based superalloy M247LC SX. Materials Science & Engineering A: Structural Materials: Properties, Microstructure and Processing, 2012, 550, 254-262.	5.6	52
26	Entropy Determination of Single-Phase High Entropy Alloys with Different Crystal Structures over a Wide Temperature Range. Entropy, 2018, 20, 654.	2.2	49
27	Neutron scattering experiments with a nickel base superalloy part I: Material and experiment. Scripta Metallurgica Et Materialia, 1994, 31, 285-290.	1.0	43
28	Neutron scattering experiments with a nickel base superalloy part II: Analysis of intensity profiles. Scripta Metallurgica Et Materialia, 1994, 31, 291-296.	1.0	43
29	Influence of W, Mo and Ti trace elements on the phase separation in Al8Co17Cr17Cu8Fe17Ni33 based high entropy alloy. Ultramicroscopy, 2015, 159, 265-271.	1.9	43
30	Mechanical characterisation of interpenetrating network metal–ceramic composites. Materials Science & Engineering A: Structural Materials: Properties, Microstructure and Processing, 2010, 527, 1260-1265.	5.6	42
31	Molecular Deformation Mechanisms in UHMWPE During Tribological Loading in Artificial Joints. Tribology Letters, 2010, 38, 1-13.	2.6	41
32	Characterisation of novel precursor-derived ceramic coatings with glass filler particles on steel substrates. Surface and Coatings Technology, 2012, 207, 319-327.	4.8	41
33	First creep results on thin-walled single-crystal superalloys. Materials Science & Engineering A: Structural Materials: Properties, Microstructure and Processing, 2009, 510-511, 307-311.	5.6	40
34	Influence of zirconium content on microstructure and creep properties of Mo–9Si–8B alloys. Intermetallics, 2014, 48, 3-9.	3.9	39
35	Creep Resistance and Oxidation Behavior of Novel Mo-Si-B-Ti Alloys. Jom, 2015, 67, 2621-2628.	1.9	36
36	Analysis of matrix and interfacial dislocations in the nickel base superalloy CMSX-4 after creep in [1̄11] direction. Scripta Metallurgica Et Materialia, 1994, 31, 1481-1486.	1.0	34

#	Article	IF	CITATIONS
37	Investigation of near surface structure in order to determine process-temperatures during different machining processes of Ti6Al4V. Scripta Materialia, 2004, 50, 121-126.	5.2	34
38	Microstructure and dislocation configurations in fatigued [001] specimens of the nickel-based superalloy CMSX-6. Scripta Metallurgica Et Materialia, 1991, 25, 1845-1850.	1.0	33
39	Abrasion resistance of oxidized zirconium in comparison with CoCrMo and titanium nitride coatings for artificial knee joints. Journal of Biomedical Materials Research - Part B Applied Biomaterials, 2010, 93B, 244-251.	3.4	33
40	Microstructure and Mechanical Properties of Precipitate Strengthened High Entropy Alloy Al10Co25Cr8Fe15Ni36Ti6 with Additions of Hafnium and Molybdenum. Entropy, 2019, 21, 169.	2.2	33
41	Zr diffusion in BCC refractory high entropy alloys: A case of â€~non-sluggish' diffusion behavior. Acta Materialia, 2022, 233, 117970.	7.9	33
42	Numerical Determination of Secondary Dendrite Arm Spacing for IN738LC Investment Castings. Metallurgical and Materials Transactions A: Physical Metallurgy and Materials Science, 2011, 42, 1847-1853.	2.2	32
43	Influence of Solid Solution Hardening on Creep Properties of Single-Crystal Nickel-Based Superalloys. Metallurgical and Materials Transactions A: Physical Metallurgy and Materials Science, 2015, 46, 1125-1130.	2.2	32
44	Microstructure, oxidation resistance and high-temperature strength of γ′ hardened Pt-base alloys. Intermetallics, 2007, 15, 539-549.	3.9	31
45	High-temperature oxidation behaviour of a single-phase (Mo,Ti)5Si3 (Mo–Si–Ti) alloy. Scripta Materialia, 2012, 66, 223-226.	5.2	31
46	Material model describing the orientation dependent creep behavior of single crystals based on dislocation densities of slip systems. International Journal of Plasticity, 1999, 15, 285-298.	8.8	30
47	A TEM investigation of the γ/γ′ phase boundary in Pt-based superalloys. Jom, 2005, 57, 49-51.	1.9	29
48	Potential for adhesive wear in friction couples of UHMWPE running against oxidized zirconium, titanium nitride coatings, and cobaltâ€chromium alloys. Journal of Biomedical Materials Research - Part B Applied Biomaterials, 2010, 93B, 468-475.	3.4	29
49	On the development and investigation of quaternary Pt-based superalloys with Ni additions. Metallurgical and Materials Transactions A: Physical Metallurgy and Materials Science, 2005, 36, 567-575.	2.2	28
50	Evaluating strength at ultra-high temperatures—Methods and results. Materials Science & Engineering A: Structural Materials: Properties, Microstructure and Processing, 2008, 483-484, 587-589.	5.6	27
51	Creep properties beyond 1100°C and microstructure of Co–Re–Cr alloys. Materials Science & Engineering A: Structural Materials: Properties, Microstructure and Processing, 2010, 528, 650-656.	5.6	27
52	Tensile creep behavior of HfNbTaTiZr refractory high entropy alloy at elevated temperatures. Acta Materialia, 2022, 237, 118188.	7.9	27
53	Effect of W on tempering behaviour of a 3Â%Co modified P92 steel. Journal of Materials Science, 2016, 51, 9424-9439.	3.7	26
54	Microstructural analysis of Ta-containing NiCoCrAlY bond coats deposited by HVOF on different Ni-based superalloys. Surface and Coatings Technology, 2018, 354, 214-225.	4.8	26

#	Article	IF	CITATIONS
55	Dislocation energies for an anisotropic cubic crystal calculations and observations for NiAl. Philosophical Magazine A: Physics of Condensed Matter, Structure, Defects and Mechanical Properties, 1993, 67, 307-323.	0.6	25
56	High-Temperature Oxidation Behavior of Two Nickel-Based Superalloys Produced by Metal Injection Molding for Aero Engine Applications. Metallurgical and Materials Transactions A: Physical Metallurgy and Materials Science, 2014, 45, 4561-4571.	2.2	24
57	Pt-Al-Cr-Ni superalloys: Heat treatment and microstructure. Jom, 2004, 56, 40-43.	1.9	23
58	Tensile Behavior and Evolution of the Phases in the Al10Co25Cr8Fe15Ni36Ti6 Compositionally Complex/High Entropy Alloy. Entropy, 2018, 20, 646.	2.2	23
59	Phase-Field Modeling of Precipitation Growth and Ripening During Industrial Heat Treatments in Ni-Base Superalloys. Metallurgical and Materials Transactions A: Physical Metallurgy and Materials Science, 2018, 49, 4146-4157.	2.2	23
60	High entropy alloy nanocomposites produced by high pressure torsion. Acta Materialia, 2021, 208, 116714.	7.9	21
61	High- temperature deformation properties of nial single crystals. Metallurgical and Materials Transactions A: Physical Metallurgy and Materials Science, 1996, 27, 1229-1240.	2.2	20
62	Fast Internal Oxidation of Ni–Zr–Y Alloys at Low Oxygen Pressure. Oxidation of Metals, 2004, 61, 239-251.	2.1	20
63	High temperature (salt melt) corrosion tests with ceramic-coated steel. Materials Chemistry and Physics, 2015, 159, 10-18.	4.0	20
64	Phase-field modeling of γ/γ″ microstructure formation in Ni-based superalloys with high γ″ volume fraction. Intermetallics, 2020, 120, 106745.	3.9	20
65	Sub-picosecond single-pulse laser ablation of the CrMnFeCoNi high entropy alloy and comparison to stainless steel AISI 304. Applied Surface Science, 2021, 544, 148839.	6.1	20
66	Towards superior high temperature properties in low density ferritic AlCrFeNiTi compositionally complex alloys. Acta Materialia, 2021, 216, 117113.	7.9	20
67	Configuration of superdislocations in the γ′-Pt3Al phase of a Pt-based superalloy. Intermetallics, 2014, 48, 71-78.	3.9	19
68	Laser Cladding of Ultra-Thin Nickel-Based Superalloy Sheets. Materials, 2017, 10, 279.	2.9	19
69	Improving the oxidation resistance of Cr-Si-based alloys by ternary alloying. Corrosion Science, 2020, 165, 108376.	6.6	19
70	Orientation-dependent creep behavior and microstructure of nickel solid solution single crystals. Acta Materialia, 1999, 47, 397-406.	7.9	18
71	Atomic site location by channelling enhanced microanalysis (ALCHEMI) in γ′-strengthened Ni- and Pt-base alloys. Acta Materialia, 2008, 56, 4267-4276.	7.9	18
72	Evolution of γ/γ' phases, their misfit and volume fractions in Al10Co25Cr8Fe15Ni36Ti6 compositionally complex alloy. Materials Characterization, 2019, 154, 363-376.	4.4	18

#	Article	IF	CITATIONS
73	Internal oxidation with significant contribution of oxygen diffusion through the oxide phase. Corrosion Science, 2012, 63, 187-192.	6.6	17
74	Reasons for Volume Contraction after Longâ€Term Annealing of Waspaloy. Advanced Engineering Materials, 2015, 17, 1106-1112.	3.5	17
75	3D printed polymer positive models for the investment casting of extremely thin-walled single crystals. Journal of Materials Processing Technology, 2021, 293, 117095.	6.3	17
76	Hysteretic Heating During Cyclic Loading of Medical Grade Ultra High Molecular Weight Polyethylene (UHMWPE). Advanced Engineering Materials, 2007, 9, 1089-1096.	3.5	15
77	Development of a precipitation-strengthened Pt-base superalloy. Materials Science & Engineering A: Structural Materials: Properties, Microstructure and Processing, 2009, 510-511, 328-331.	5.6	15
78	Creep behavior of polycrystalline and single crystal Ni-based superalloys coated with Ta-containing NiCoCrAlY by high-velocity oxy-fuel spraying. Scripta Materialia, 2020, 178, 522-526.	5.2	15
79	Uniaxial mechanical properties of face-centered cubic single- and multiphase high-entropy alloys. MRS Bulletin, 2022, 47, 168-174.	3.5	15
80	Anisotropie creep behavior of a nickel-based superalloy compared with single phase nickel solid solution and γ′ phase single crystals. Materials Science & Engineering A: Structural Materials: Properties, Microstructure and Processing, 1997, 234-236, 237-241.	5.6	14
81	Determination of solubility limits of refractory elements in TCP phases of the Ni-Mo-Cr ternary system using diffusion multiples. Journal of Alloys and Compounds, 2019, 788, 67-74.	5.5	14
82	Determination of Oxygen Diffusion Along Nickel/Zirconia Phase Boundaries by Internal Oxidation. Oxidation of Metals, 2012, 77, 149-165.	2.1	12
83	Strengthened Cr-Si-base alloys for high temperature applications. International Journal of Refractory Metals and Hard Materials, 2018, 76, 72-81.	3.8	12
84	Phase-field modeling of γ′-precipitate shapes in nickel-base superalloys and their classification by moment invariants. European Physical Journal B, 2019, 92, 1.	1.5	12
85	Enrichment of boron at grain boundaries of platinum-based alloys determined by electron energy loss spectroscopy in a transmission electron microscope. International Journal of Materials Research, 2010, 101, 577-579.	0.3	11
86	Microstructural study of boron-doped Co–Re–Cr alloys by means of transmission electron microscopy and electron energy-loss spectroscopy. International Journal of Materials Research, 2012, 103, 554-558.	0.3	11
87	On the interaction between γ′′ precipitates and dislocation microstructures in Nb containing single crystal nickel-base alloys. Materials Characterization, 2020, 165, 110389.	4.4	11
88	Influence of high melting elements on microstructure, tensile strength and creep resistance of the compositionally complex alloy Al10Co25Cr8Fe15Ni36Ti6. Materials Chemistry and Physics, 2021, 274, 125163.	4.0	11
89	Creep properties of Ni3(AlTiTa) γ′ phase single crystals. Metallurgical and Materials Transactions A: Physical Metallurgy and Materials Science, 2000, 31, 1733-1740.	2.2	10
90	Finite-element modelling of anisotropic single-crystal superalloy creep deformation based on dislocation densities of individual slip systems. International Journal of Materials Research, 2005, 96, 595-601.	0.8	10

#	Article	IF	CITATIONS
91	Determination of the temperature rise within UHMWPE tibial components during tribological loading. Acta Biomaterialia, 2010, 6, 552-562.	8.3	10
92	Influence of casting surface on creep behaviour of thin-wall Ni-base superalloy Inconel100. Journal of Materials Processing Technology, 2013, 213, 722-727.	6.3	10
93	Temperature Dependent Solid Solution Strengthening in the High Entropy Alloy CrMnFeCoNi in Single Crystalline State. Metals, 2020, 10, 1412.	2.3	10
94	Optimization of composition and heat treatment of age-hardened Ptâ^'Alâ^'Crâ^'Ni alloys. Metallurgical and Materials Transactions A: Physical Metallurgy and Materials Science, 2005, 36, 681-689.	2.2	9
95	Determination of phases in the system chromium–platinum (Cr–Pt) and thermodynamic calculations. Materials Science & Engineering A: Structural Materials: Properties, Microstructure and Processing, 2009, 510-511, 322-327.	5.6	9
96	Synthesis and characterization of a Pt–Al–Cr–Ni γ/γ′-coating on the Ni-based superalloy CMSXâ€4. Su and Coatings Technology, 2013, 236, 347-352.	rfaçe 4.8	8
97	Temperature evolution of lattice misfit in Hf and Mo variations of the Al10Co25Cr8Fe15Ni36Ti6 compositionally complex alloy. Scripta Materialia, 2020, 188, 74-79.	5.2	8
98	An Enhanced Three-Step Oxidation Process to Improve Oxide Adhesion on Zirconium Alloys. Oxidation of Metals, 2014, 82, 99-112.	2.1	7
99	Determination of heat treatment parameters by experiments and CALPHAD for precipitate hardening of Cr-Alloys with Si, Ge and Mo. Intermetallics, 2020, 116, 106636.	3.9	7
100	Quantification of Solid Solution Strengthening and Internal Stresses through Creep Testing of Ni-Containing Single Crystals at 980 A°C. Metals, 2021, 11, 1130.	2.3	7
101	Anisotropic Growth of the Primary Dendrite Arms in a Singleâ€Crystal Thinâ€Walled Nickelâ€Based Superalloy. Advanced Engineering Materials, 2022, 24, .	3.5	7
102	Elemental effects on the oxidation of refractory compositionally complex alloys. International Journal of Refractory Metals and Hard Materials, 2022, 108, 105918.	3.8	7
103	The effects of Ta additions on the phase compositions and high temperature properties of Pt base alloys. Materials Science & Engineering A: Structural Materials: Properties, Microstructure and Processing, 2008, 479, 306-312.	5.6	6
104	Transition from internal to external oxidation in binary Ni–Zr and ternary Ni–Zr–Y alloys. Corrosion Science, 2015, 94, 218-223.	6.6	6
105	Oxygen diffusion kinetics of an advanced three step heat treatment for zirconium alloy ZrNb7. Surface and Coatings Technology, 2018, 339, 139-146.	4.8	6
106	Phase-Field Modeling of γ′ and γ″ Precipitate Size Evolution During Heat Treatment of Ni-Based Superalloys. Minerals, Metals and Materials Series, 2020, , 500-508.	0.4	6
107	Thermo-physical properties of Hastelloy X and Haynes 214 close to the melting range. Materials Science and Technology, 2020, 36, 1012-1019.	1.6	5
108	Discontinuities in Oxidation Kinetics: A New Model and its Application to Cr–Si-Base Alloys. Oxidation of Metals, 2021, 95, 445-465.	2.1	5

#	Article	IF	CITATIONS
109	Development and evaluation of an image processing algorithm for monitoring fiber laser fusion cutting by a high-speed camera. Journal of Laser Applications, 2021, 33, 032004.	1.7	5
110	Effect of Wall Thickness and Surface Conditions on Creep Behavior of a Single-Crystal Ni-Based Superalloy. Metals, 2022, 12, 1081.	2.3	5
111	Tailored platinum-nickel nanostructures on zirconia developed by metal casting, internal oxidation and dealloying. Corrosion Science, 2016, 112, 246-254.	6.6	4
112	Quantitative analysis of Mo–Si–B alloy phases with wavelength dispersive spectroscopy (WDS–SEM). X-Ray Spectrometry, 2018, 47, 153-158.	1.4	4
113	Stainless steel powder produced by a novel arc spray process. Journal of Materials Research and Technology, 2020, 9, 8314-8322.	5.8	4
114	High-Entropy Alloys: Balancing Strength and Ductility at Room Temperature. , 2022, , 441-453.		4
115	Simulation of the Î,′ Precipitation Process with Interfacial Anisotropy Effects in Al-Cu Alloys. Materials, 2021, 14, 1280.	2.9	4
116	Oxygen diffusion hardened zirconium alloy ZrNb7 – Tribological properties derived from Calo wear and wheel on flat experiments. Tribology International, 2022, 165, 107304.	5.9	4
117	Control of ultrafast laser ablation efficiency by stress confinement due to strong electron localization in high-entropy alloys. Applied Surface Science, 2022, 594, 153427.	6.1	4
118	Comparison of oxide measurement techniques applied to Ti6Al4V. Materials Characterization, 2005, 55, 153-159.	4.4	3
119	A novel method for the preparation of porous zirconia ceramics with multimodal pore size distribution. Journal of the European Ceramic Society, 2014, 34, 1311-1319.	5.7	3
120	Influence of Ingot and Powder Metallurgy Production Route on the Tensile Creep Behavior of Mo–9Si–8B Alloys with Additions of Al and Ge. Advanced Engineering Materials, 2018, 20, 1700751.	3.5	3
121	Optimisation of a Jewellery Platinum Alloy for Precision Casting: Evaluation of Mechanical, Microstructural and Optical Properties. Johnson Matthey Technology Review, 2018, 62, 364-382.	1.0	3
122	On the Formation of Eutectics in Variations of the Al10Co25Cr8Fe15Ni36Ti6 Compositionally Complex Alloy. Metallurgical and Materials Transactions A: Physical Metallurgy and Materials Science, 2021, 52, 143-150.	2.2	3
123	Quantitative Shape-Classification of Misfitting Precipitates during Cubic to Tetragonal Transformations: Phase-Field Simulations and Experiments. Materials, 2021, 14, 1373.	2.9	3
124	The Influence of Oxide Color on the Surface Characteristics of Zirconium Alloy ZrNb7 (wt%) After Different Heat Treatments. Oxidation of Metals, 2021, 95, 377-388.	2.1	3
125	Improving the Adhesion of a Hard Oxide Layer on Ti6Al4V by a Threeâ€Step Thermal Oxidation Process. Advanced Engineering Materials, 2022, 24, 2100864.	3.5	3
126	Electron energy losses by channelling-enhanced microanalysis in a γ′-strengthened Ni-base alloy with Ti additions. Acta Materialia, 2009, 57, 4217-4223.	7.9	2

#	Article	IF	CITATIONS
127	Microstructural and micromechanical characterisation of a Pt–Al–Cr–Ni–Re alloy by means of transmission electron microscopy and nanoindentation. International Journal of Materials Research, 2010, 101, 585-588.	0.3	2
128	Near‣urface Microstructural Reorganization of UHMWPE under Cyclic Load – A Pilot Study. Advanced Engineering Materials, 2011, 13, B476.	3.5	2
129	Tensile Creep Properties of Cr-Si Alloys at 980 °C in Air—Influence of Ge and Mo Addition. Metals, 2021, 11, 1072.	2.3	2
130	Consistent Quantification of Precipitate Shapes and Sizes in Two and Three Dimensions Using Central Moments. Integrating Materials and Manufacturing Innovation, 2022, 11, 159-171.	2.6	2
131	Internal Oxidation of Ternary Alloys Forming a High Oxygen Conductive Oxide. Oxidation of Metals, 2016, 86, 193-203.	2.1	0
132	The influence of Cr, Al, Co, Fe and C on negative creep of Waspaloy. International Journal of Materials Research, 2021, 112, 90-97.	0.3	0
133	Measurement of the lattice misfit of Pt–Al–Cr superalloy by convergent beam electron diffraction (CBED). International Journal of Materials Research, 2010, 101, 580-584.	0.3	0
134	Determination of the local oxygen distribution in a commercial titanium alloy by 3-dimensional atom probe. International Journal of Materials Research, 2022, 94, 771-773.	0.3	0

9